A Darier disease mutation relieves kinetic constraints imposed by the tail of sarco(endo)plasmic reticulum Ca^{2+}-ATPase 2b

Received for publication, November 13, 2017, and in revised form, January 19, 2018 Published, Papers in Press, January 23, 2018, DOI 10.1074/jbc.RA117.000941

Stine A. Mikkelsen[‡], **Peter Vangheluwe**[§], **and Jens Peter Andersen**[‡1]

From the [‡]*Department of Biomedicine, Aarhus University, DK-8000 Aarhus C, Denmark and the* [§]*Department of Cellular and Molecular Medicine, KU Leuven, B-3000 Leuven, Belgium*

Edited by Roger J. Colbran

The sarco(endo)plasmic reticulum Ca^{2+}-ATPase (SERCA) 2b isoform possesses an extended C terminus (SERCA2b tail) forming an 11th transmembrane (TM) helix, which slows conformational changes of the Ca^{2+}-pump reaction cycle. Here, we report that a Darier disease (DD) mutation of SERCA2b that changes a glutamate to a lysine in the cytoplasmic loop between TM8 and TM9 (E917K) relieves these kinetic constraints. We analyzed the effects of this mutation on the overall reaction and the individual partial reactions of the Ca^{2+} pump compared with the corresponding mutations of the SERCA2a and SERCA1a isoforms, lacking the SERCA2b tail. In addition to a reduced affinity for Ca^{2+}, caused by the mutation in all three isoforms examined, we observed a unique enhancing effect on the turnover rates of ATPase activity and Ca^{2+} transport for the SERCA2b E917K mutation. This relief of kinetic constraints contrasted with inhibitory effects observed for the corresponding SERCA2a and SERCA1a (E918K) mutations. These observations indicated that the E917K/E918K mutations affect the rate-limiting conformational change in isoform-specific ways and that the SERCA2b mutation perturbs the interactions of TM11 with other SERCA2b regions. Mutational analysis of an arginine in TM7 that interacts with the glutamate in SERCA1a crystal structures suggested that in wildtype SERCA2b, the corresponding arginine (Arg-835) may be involved in mediating the conformational restriction by TM11. Moreover, the E917K mutation may disturb TM11 through the cytoplasmic loop between TM10 and TM11. In conclusion, our findings have identified structural elements of importance for the kinetic constraints imposed by TM11.

Sarco(endo)plasmic reticulum Ca^{2+}-ATPases (SERCAs)[2] create and maintain Ca^{2+} gradients essential to cellular Ca^{2+} homeostasis and Ca^{2+} signaling (1, 2). SERCAs belong to the P-type ATPase family of membrane pumps that utilize ATP through transient phosphorylation of a conserved aspartic acid residue (3–6). Three SERCA genes, *ATP2A1*, *ATP2A2*, and *ATP2A3*, encode the proteins SERCA1, SERCA2, and SERCA3, each of which are found in alternatively spliced forms, thus resulting in multiple SERCA isoforms (SERCA1a and -b, SERCA2a–d, and SERCA3a–f) with distinct expression profiles and kinetic properties (2, 7–15). All the SERCA isoforms appear to pump Ca^{2+} into the lumen of the sarco(endo)plasmic reticulum at a stoichiometry of 2 Ca^{2+} per ATP hydrolyzed, returning 2 or possibly 3 protons (indicated as *n* in Scheme 1, due to the uncertainty about the exact number and its possible variability (16)). During its enzymatic cycle, which is prototypical of P-type ATPases (6), SERCA appears in four different major conformational states, E_1, E_1P, E_2P, and E_2 (P indicates phosphorylation, see Scheme 1). Structural information at atomic resolution is available only for SERCA1a, which was the first P-type ATPase to be crystallized and examined by X-ray diffraction (17). P-type ATPases are generally made up of three cytoplasmic domains: P (phosphorylation domain, contains the phosphorylated aspartic acid residue); N (nucleotide-binding domain), and A (actuator domain). The transmembrane sector consists of 6–12 helical segments, whose movements, leading to substrate translocation across the membrane, are coupled with the movements of the cytoplasmic domains, resulting in a coordinated ATP hydrolysis and substrate translocation (4–6). Although the SERCA proteins generally possess 10 transmembrane helical segments (TM1–TM10), the ubiquitously expressed "housekeeping" isoform SERCA2b is unique by its extended C terminus forming an 11th transmembrane helix (TM11) with a luminal extension (LE), collectively referred to as the SERCA2b tail (18–20). The preceding amino acid sequence of SERCA2b is identical to SERCA2a and 85% identical to SERCA1a. The X-ray diffraction analysis of SERCA1a in conjunction with site-directed mutagenesis studies has defined six residues with oxygen-containing side chains in the transmembrane segments TM4, TM5, TM6, and TM8 as Ca^{2+} ligands at two high-affinity Ca^{2+} transport sites (17, 21–24). These residues are conserved among the SERCA isoforms, and therefore all are believed to possess Ca^{2+}-binding sites similar to those of SERCA1a. However, many other residues contribute to define the Ca^{2+}-binding properties, which differ significantly between some of the isoforms. In particular, SERCA3

This work was supported in part by the Danish Medical Research Council, the Novo Nordisk Foundation, and the Lundbeck Foundation, Denmark (to J. P. A.). The authors declare that they have no conflicts of interest with the contents of this article.

This article was selected as one of our Editors' Picks.

[1] To whom correspondence should be addressed: Dept. of Biomedicine, Aarhus University, Ole Worms Allé 4, Bldg. 1160, DK-8000 Aarhus C, Denmark. E-mail: jpa@biomed.au.dk.

[2] The abbreviations used are: SERCA, sarco(endo)plasmic reticulum Ca^{2+}-ATPase; Ca^{2+}-ATPase, Ca^{2+}-transporting ATPase; DD, Darier disease; LE, 11-amino acid-luminal extension; TES, 2-{[(2-hydroxy-1,1-bis(hydroxymethyl)ethyl]amino}ethanesulfonic acid; TM1–TM11, 11 transmembrane segments numbered from the N-terminal end of the protein.

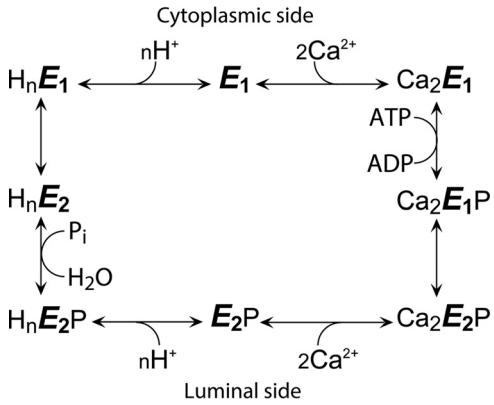

SCHEME 1. **SERCA reaction cycle.** The major enzyme conformations are indicated as E_1 and E_2. *P* indicates phosphorylation at the conserved P-domain aspartic acid residue. Two Ca^{2+} ions are transported in each enzyme cycle. The proton counter transport is indicated here and throughout the text by H_n, where *n* most likely is 2 at physiological pH, but may vary dependent on pH (16).

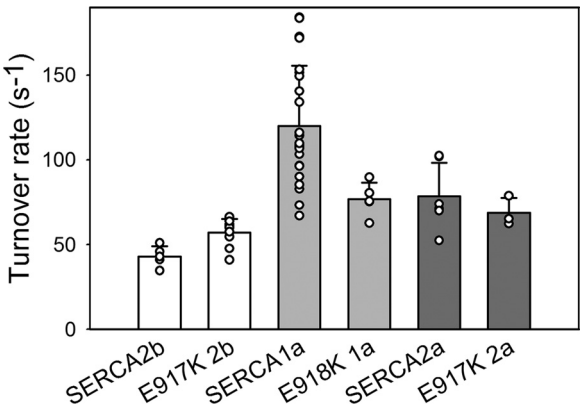

Figure 1. Maximal turnover rate of ATPase activity. The maximal ATPase activity was determined at 37 °C in medium containing 50 mM TES/Tris (pH 7.0), 105 mM KCl, 4.5 mM ATP, 6.25 mM $MgCl_2$, 0.89 mM EGTA, 2 μM Ca^{2+} ionophore A23187, and the $CaCl_2$ concentration required to obtain maximal activity (*cf.* Fig. 2). The turnover rate was calculated relative to the active-site concentration determined by phosphorylation under stoichiometric conditions. All the individual data points collected are shown as *circles*, and the *height of the columns* show the average values. The vertical distance between the *top of the column* and the *horizontal error bars* indicates the S.D.; for further information on statistics, see Table 1.

enzymes exhibit lower Ca^{2+} affinity than SERCA1a (14), whereas SERCA2b exhibits higher Ca^{2+} affinity than both SERCA1a and SERCA2a (15, 18–20). SERCA2b is furthermore characterized by significantly lower rates of the major rate-limiting conformational changes of the enzyme cycle compared with the other isoforms, which may be ascribed to the presence of the SERCA2b tail (15, 20).

SERCA2b is the predominant isoform in the human skin (25, 26). A variety of mutations in SERCA2b have been found to result in Darier disease (DD), an autosomal dominant skin disorder characterized by dyskeratosis and acantholysis, often associated with neuropsychiatric abnormality (26–30). The skin manifestations seem to be caused by abnormal differentiation of the keratinocytes and lack of desmosomes between keratinocytes due to depletion of endoplasmic reticulum Ca^{2+} stores with resulting apoptosis and change of the Ca^{2+} gradient normally existing across the epidermal layers (26, 31).

In this study, we have analyzed the functional consequences of the DD mutation E917K, which targets a glutamate located in the cytoplasmic loop between TM8 and TM9 (32). We unexpectedly found this mutation to relieve the kinetic constraints normally imposed by the SERCA2b tail. To understand the role of the SERCA2b tail in the functional effects of the SERCA2b E917K mutation, we replaced the corresponding residue in SERCA2a (E917K) and SERCA1a (E918K and E918A), which do not possess the tail characteristic of SERCA2b. Furthermore, we studied the effects of alanine mutations of Arg-835 in SERCA2a/2b and Arg-836 in SERCA1a, as this arginine residue, located in TM7, interacts with Glu-918 in the crystal structures of SERCA1a. The results demonstrate the importance of both Glu-917 and Arg-835 of SERCA2b in mediating the kinetic effects of the SERCA2b tail.

Results

Expression level, maximal activity, and Ca^{2+} dependence of SERCA2a and SERCA2b E917K and SERCA1a E918K and E918A mutants

Because COS-1 cells contain little endogenous SERCA, they are ideal for expression and functional studies of SERCA isoforms and mutants (8, 11, 15, 18, 21) and were used here. First, we examined DD mutation E917K in SERCA2b (human) and the corresponding mutations E917K in SERCA2a (human) and E918K in SERCA1a (rabbit). The expression levels of these mutants in the COS-1 cells were significantly lower than the expression levels of the respective wildtypes, and more so for the SERCA2 mutants (~5- and 10-fold reduced for SERCA2b and SERCA2a, respectively) than for the SERCA1a mutant (2-fold reduced). ATPase activity and Ca^{2+} transport measurements presented below were corrected for expression level by calculating the turnover rates (molecular rates, *i.e.* rate of ATP hydrolysis or Ca^{2+} transport per active enzyme). In agreement with previous findings (11, 15, 20), the present data show that the maximal turnover rate of ATPase activity of wildtype SERCA2b is only about one-third that of the SERCA1a wildtype, and the same is the case for the maximal turnover rate of the ATP-dependent active Ca^{2+} uptake in the microsomal vesicles determined under conditions of saturation of the high-affinity Ca^{2+}-binding sites (5 μM free Ca^{2+}, Fig. 1, and Table 1). SERCA2a showed maximal rates intermediate between those of SERCA2b and SERCA1a, also in good agreement with the previous findings (15, 20). This difference between the wildtypes illustrates the kinetic constraints imposed on SERCA2b by its tail. Unexpectedly, the present results with the mutants revealed that the maximal turnover rate of the ATPase activity of DD mutant SERCA2b E917K is 1.3-fold higher than that of the SERCA2b wildtype, whereas the corresponding SERCA1a E918K mutant showed a significant 1.6-fold reduction of the maximal turnover rate of ATPase activity relative to wildtype SERCA1a. A similar difference between the effects of the corresponding mutations in SERCA2b and SERCA1a was noted for the turnover rate of Ca^{2+} transport, being 1.5-fold enhanced for E917K in SERCA2b and reduced as much as 2.5-fold for E918K in SERCA1a, relative to the corresponding wildtype (Table 1). Thus, the inhibition of the SERCA2b wildtype relative to the SERCA1a wildtype is relieved by the E917K mutation

Table 1
Expression and characteristics of the overall ATPase and Ca^{2+} transport reactions
Average values from *n* independent experiments are reported ± S.D.

	Expression[a]	*n*	Turnover ATPase[b]	*n*	Turnover Ca^{2+} uptake[c]	*n*	Ca^{2+} affinity[d]	*n*	Vanadate affinity[e]	*n*
	%		s^{-1}		min^{-1}		μM		μM	
SERCA1a										
WT	100 ± 46	67	120 ± 36	24	751 ± 496	11	0.31 ± 0.04	13	49 ± 6.2	12
E918K	45 ± 9.6	5	77 ± 9.9	5	300 ± 74	5	0.82 ± 0.13	4	7.9 ± 3.3	5
E918A	65 ± 16	4	87 ± 9.7	5	245 ± 21	4	0.46 ± 0.05	4	19 ± 2.0	3
R836A	5.9 ± 3.8	11	162 ± 55	7	760 ± 162	11	0.48 ± 0.05	3	2.0 ± 0.75	3
SERCA2b										
WT	100 ± 60	6	43 ± 6.0	5	226 ± 144	4	0.12 ± 0.02	5	27 ± 4.6	4
E917K	18 ± 11	9	57 ± 8.2	9	349 ± 158	4	0.44 ± 0.12	6	10 ± 9.1	3
R835A	17 ± 7.7	7	72 ± 12	2	803 ± 203	5	0.27 ± 0.03	3	2.0 ± 0.45	2
SERCA2a										
WT	100 ± 59	13	79 ± 20	6	650 ± 216	13	0.21 ± 0.01	3	7.6 ± 1.1	3
E917K	12 ± 5.7	6	69 ± 8.8	3	511 ± 61	4	1.00 ± 0.39	5	3.2 ± 0.78	2
R835A	7.7 ± 4.9	4	101 ± 16	4	709 ± 130	4	0.55 ± 0.28	3	4.4 ± 5.0	2

[a] Expression levels (shown relative to the corresponding wildtype) were determined by measuring the level of phosphorylation under stoichiometric conditions (see "Experimental procedures").
[b] Maximal turnover rate of ATPase activity (mol of phosphate liberated/s/mol of enzyme expressed).
[c] Maximal turnover rate of Ca^{2+} transport (mol of Ca^{2+} taken up in microsomes/min/mol of enzyme expressed). Note that turnover rates of ATPase activity and Ca^{2+} transport were determined under different conditions (see "Experimental procedures") and therefore are comparable only on a relative basis relating the values to that of the corresponding wildtype.
[d] The $K_{0.5}$ value for Ca^{2+} activation was determined by curve fitting as described in the legend to Fig. 2.
[e] The $K_{0.5}$ value for vanadate inhibition was determined by curve fitting as described in the legend to Fig. 3.

in SERCA2b. A relation of this finding to the presence of the SERCA2b tail (TM11 plus LE) was revealed by the data obtained with the SERCA2a E917K mutant and wildtype, which do not possess the SERCA2b tail but are otherwise identical to mutant and wildtype SERCA2b. In the SERCA2a protein environment, the mutation was inhibitory similar to the finding with SERCA1a, although to a lesser extent (Fig. 1 and Table 1), thus indicating that the activation seen for SERCA2b E917K is the consequence of a change of the interaction of the SERCA2b tail, relieving its inhibitory influence.

In contrast to the differential effects of the E917K/E918K mutation on the maximal turnover rates in the three isoforms, the mutation exerted similar effects on the Ca^{2+} activation profiles of the three isoforms studied, reducing the apparent Ca^{2+} affinity in all cases (Fig. 2 and Table 1, $K_{0.5}$ 3.7-, 2.6-, and 4.8-fold increased for SERCA2b E917K, SERCA1a E918K, and SERCA2a E917K, respectively, relative to wildtype, where $K_{0.5}$ is the ligand concentration giving half-maximum effect).

The effects of the SERCA1a E918A mutation were also characterized. Like mutant E918K, E918A showed a significantly reduced maximal rate and reduced apparent Ca^{2+} affinity, although the affinity decrease was less pronounced compared with E918K (Table 1).

Vanadate sensitivity of SERCA2a and SERCA2b E917K and SERCA1a E918K and E918A mutants

Vanadate is an analog of the phosphoryl group in the transition state occurring during dephosphorylation of H_nE_2P (*cf.* Scheme 1). Therefore, it binds strongly to P-type ATPases in the E_2 conformation, inhibiting the ATPase activity (33, 34). SERCA2a and SERCA2b E917K showed 2–3-fold increase of the apparent vanadate affinity for inhibition of steady-state ATPase activity (reduced $K_{0.5}$) compared with the corresponding wildtypes. The SERCA1a E918K and E918A mutants likewise showed increased apparent vanadate affinity, as much as 6–7-fold for E918K (Fig. 3 and Table 1). Because vanadate binds to E_2 states of the enzyme and not to E_1 states, the

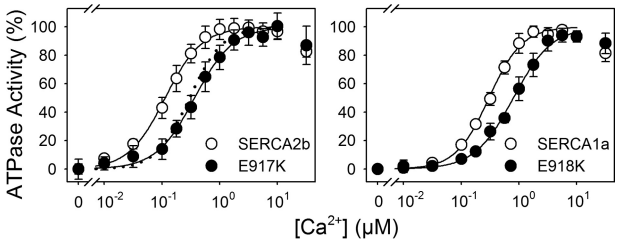

Figure 2. Ca^{2+} dependence of ATPase activity. The ATPase activity was determined at 37 °C in medium containing 50 mM TES/Tris (pH 7.0), 105 mM KCl, 4.5 mM ATP, 6.25 mM $MgCl_2$, 0.89 mM EGTA and varying concentrations of $CaCl_2$ to give the indicated concentrations of free Ca^{2+} and 2 μM of the Ca^{2+} ionophore A23187. *Error bars* (seen only when larger than the size of the symbols) indicate S.D. The *lines to the left* of the maximum are regression curves obtained by fitting the Hill equation: $V = V_{max}\cdot([Ca^{2+}]^h/(K_{0.5}{}^h + [Ca^{2+}]^h))$, where *h* is the Hill coefficient (here between 1 and 2); *V* is the ATPase activity at the given Ca^{2+} concentration, and V_{max} is the maximum ATPase activity, in the graph used to normalize the data such that the maximum is 100%. The *dotted line* represents the SERCA1a wildtype from the *right panel* for direct comparison. The extracted $K_{0.5}$ values with statistics are presented in Table 1 ("Ca^{2+} affinity").

increase of the apparent vanadate affinity may result from accumulation of H_nE_2 during enzyme turnover, which could occur as a consequence of an increased rate of formation of this intermediate through the phosphoenzyme processing steps $Ca_2E_1P \rightarrow Ca_2E_2P \rightarrow E_2P \rightarrow H_nE_2P \rightarrow H_nE_2$ and/or a slowing of the Ca^{2+}-binding reaction sequence $H_nE_2 \rightarrow H_nE_1 \rightarrow E_1 \rightarrow Ca_2E_1$ (*cf.* Scheme 1). Studies of the partial reactions described below indicate that both kinds of effects are involved here and that their relative contributions depend on the isoform.

Transient kinetics of phosphorylation of SERCA2a and SERCA2b E917K and SERCA1a E918K and E918A mutants

The transient kinetics of phosphorylation was studied at pH 7.0 and 25 °C using a Bio-Logic QFM-5 quenched-flow module for rapid mixing. Phosphorylation was initiated by mixing Ca^{2+}-saturated enzyme with 2.5 μM [γ-^{32}P]ATP. The observed phosphorylation time courses show a phosphorylation overshoot of variable size, before steady state is reached (Fig. 4). The overshoot appears because of accumulation of dephosphoen-

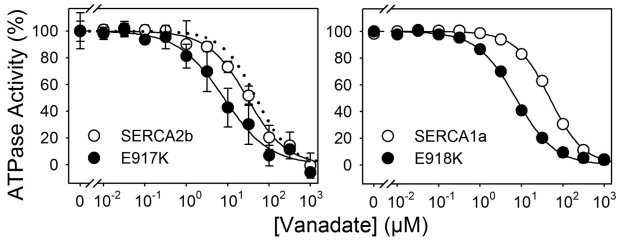

Figure 3. Vanadate dependence of ATPase activity. The ATPase activity was determined at 37 °C in medium containing 45 mM TES/Tris (pH 7.0), 105 mM KCl, 4.5 mM ATP, 6.25 mM $MgCl_2$, 0.89 mM EGTA, 1 mM $CaCl_2$ to give 50 μM of free $CaCl_2$, 2 μM of the Ca^{2+} ionophore A23187, and varying concentrations of vanadate. *Error bars* (seen only when larger than the size of the symbols) indicate S.D. A simple binding relationship was used in regression analysis of the data points: $V = V_0 \cdot (1 - [\text{vanadate}]/(K_{0.5} + [\text{vanadate}]))$, where V is the ATPase activity at the given vanadate concentration, and V_0 is the ATPase activity in the absence of vanadate, in the graph used to normalize the data such that the maximum is 100%. The *dotted line* represents the SERCA1a wild-type from the *right panel* for direct comparison. The extracted $K_{0.5}$ values with statistics are presented in Table 1 ("Vanadate affinity").

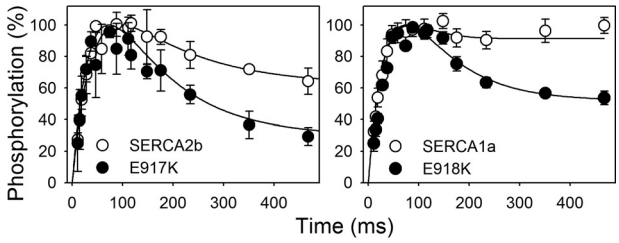

Figure 4. Transient kinetics of phosphorylation. Time course studies of the amount of phosphorylated enzyme were carried out at 25 °C using a BioLogic QFM-5 quenched-flow module. Enzyme preincubated in medium containing 40 mM MOPS/Tris (pH 7.0), 80 mM KCl, 5 mM $MgCl_2$, and 100 μM $CaCl_2$ was mixed with an equal volume of the same medium containing 5 μM [γ-^{32}P]ATP, followed by acid quenching at the indicated time intervals. In each case, the maximum phosphorylation level reached is indicated as 100%. *Error bars* (seen only when larger than the size of the symbols) indicate S.D. The lines were computed according to the simplified reaction cycle as shown in Table 2, using the SimZyme program with the rate constants indicated in Table 2.

zyme at steady state. The overshoot was minimal for the SERCA1a wildtype. The SERCA2b wildtype showed a larger overshoot, and the overshoot of SERCA2a was intermediate. For all mutants, the overshoot was larger than that of the corresponding wildtype, which is in line with the accumulation of H_nE_2 predicted from the increased vanadate sensitivity, as described above. The enzyme kinetics simulation computer software SimZyme (35) was used to estimate relevant rate constants by comparison of computed time courses with the experimental data points (Fig. 4). The computation is based on the simplified reaction cycle shown in Table 2, in which the first rate constant, k_A, represents the phosphorylation of Ca_2E_1, forming Ca_2E_1P; the second rate constant, k_B, represents the sequence of phosphoenzyme processing steps $Ca_2E_1P \rightarrow Ca_2E_2P \rightarrow E_2P \rightarrow H_nE_2P \rightarrow H_nE_2$, and the last rate constant, k_C, represents the Ca^{2+}-binding reaction sequence $H_nE_2 \rightarrow H_nE_1 \rightarrow E_1 \rightarrow Ca_2E_1$ (*cf.* Scheme 1). A lowering of k_A reduces the steepness of the rise of the phosphorylation overshoot as well as the magnitude of the overshoot, whereas the overshoot increases if k_C is reduced. The k_B, as well, has impact on the size of the overshoot, which becomes smaller with reduced k_B and larger if k_B is increased. Furthermore, the steepness of the decay phase of the overshoot increases with an increase of k_B. Because of the strong dependence of the size and shape of the overshoot

Table 2

Rate constants of partial reactions determined by computational fitting of the experimental time courses of phosphorylation

The enzyme kinetics simulation computer software "SimZyme" (35) was used to compute time courses fitting the experimental data points as shown in Fig. 4 and thereby estimate the rate constants k_A, k_B, and k_C. The simplified reaction cycle used as the basis for the computation is shown.

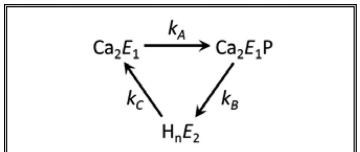

	k_A	k_B	k_C	n
	s^{-1}			
SERCA1a				
WT	27	7	17	7
E918K	27	5	3	3
E918A	27	6	7	2
R836A	27	15	6	2
SERCA2b				
WT	27	3	3	2
E917K	27	7	1.5	4
R835A	27	11	2	2
SERCA2a				
WT	27	8	5	2
E917K	27	12	2.5	2
R835A	27	11	2.5	2

on the three rate constants, there is generally not much latitude in the determination of the rate constants by curve fitting when an overshoot of significant magnitude is present. As seen in Fig. 4, good fits to the data could be obtained with a phosphorylation rate constant $k_A = 27\ s^{-1}$ for SERCA1a, SERCA2a, and SERCA2b wildtypes as well as mutants (note that due to the ATP concentration of 2.5 μM present during this experiment, the k_A value is lower than that previously determined for SERCA1a at 5 μM ATP (35 s^{-1} (35)). SERCA2a showed a small increase of k_B and a lower k_C compared with SERCA1a wildtype, and the k_B and k_C values determined for the SERCA2b wildtype were both lower than that of SERCA1a, in agreement with previous findings (15). To obtain a good fit to the data for SERCA2a E917K and SERCA2b E917K, k_B had to be increased, as much as 2.3-fold for SERCA2b E917K and 1.5-fold for SERCA2a E917K. Furthermore, k_C had to be reduced 2-fold, relative to the respective wildtypes. Hence, the above described increase of the maximal turnover rate of ATPase activity and Ca^{2+} transport induced by E917K in SERCA2b may be attributed to an increased rate of the sequence of phosphoenzyme processing steps $Ca_2E_1P \rightarrow Ca_2E_2P \rightarrow E_2P \rightarrow H_nE_2P \rightarrow H_nE_2$. For the SERCA1a E918K mutant, we found a decrease of both k_B and k_C relative to wildtype SERCA1a, which is reflected in the reduced maximal turnover rate of ATPase activity and Ca^{2+} transport of this mutant. The reduction of k_C (5.7-fold) required to fit the SERCA1a E918K data is larger than the 2-fold reduction required for E917K in SERCA2a and SERCA2b. SERCA1a E918A showed the same tendency as E918K although not as pronounced.

Rates of individual partial reactions of SERCA2b E917K and SERCA1a E918K and E918A mutants

To study more directly the mutational effect on the rate of the $Ca_2E_1P \rightarrow E_2P$ transition (*i.e.* $Ca_2E_1P \rightarrow Ca_2E_2P \rightarrow E_2P$ in

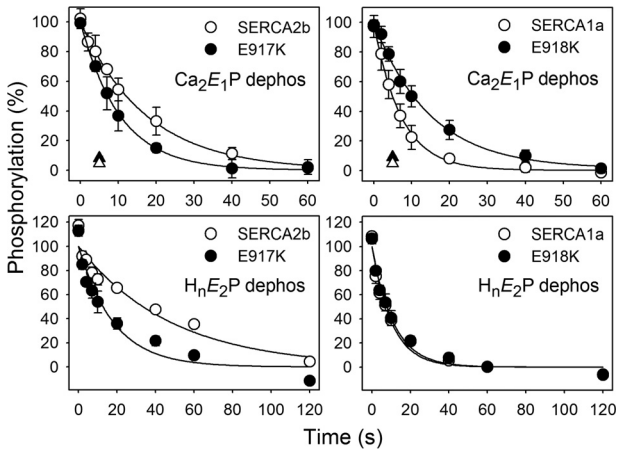

Figure 5. Kinetics of dephosphorylation of Ca_2E_1P (*upper panels*) and H_nE_2P (*lower panels*). For Ca_2E_1P dephosphorylation, the enzyme was phosphorylated for 15 s at 0 °C in medium composed from 5 μM [γ-^{32}P]ATP, 40 mM MOPS/Tris (pH 7.0), 80 mM KCl, 5 mM $MgCl_2$, 1 mM EGTA, 0.955 mM $CaCl_2$ (giving a free Ca^{2+} concentration of 10 μM), and 1.74 μM of the Ca^{2+} ionophore A23187. To follow the dephosphorylation, the phosphoenzyme was chased by removing free Ca^{2+} with EGTA added at a final concentration of 9 mM, thus preventing further phosphorylation. ADP sensitivity was demonstrated by including 1 mM ADP in the chase medium (*triangle in the lower left corner*). Acid quenching was performed at the indicated time intervals after the chase. For H_nE_2P dephosphorylation, phosphorylation was carried out at 25 °C for 10 min in medium containing 0.5 mM $^{32}P_i$, 100 mM Mes/Tris (pH 6.0), 10 mM $MgCl_2$, 2 mM EGTA, and 30% (v/v) dimethyl sulfoxide. Following cooling at 0 °C, the phosphoenzyme was chased by a 19-fold dilution with 40 mM ice-cold MOPS/Tris (pH 7.0), 10 mM KCl, 2 mM EGTA, 2 mM $MgCl_2$, and 0.5 mM non-radioactive P_i, and acid quenching was performed at the indicated time intervals after the chase. *Error bars* (seen only when larger than the size of the symbols) indicate S.D. The *lines* show the best non-linear regression fits of a monoexponential decay function $EP = EP{\cdot}e^{-k{\cdot}t}$, giving the rate constants listed with statistics in Table 3 ("$Ca_2E_1P \rightarrow E_2P$" corresponding to the *upper panels* of this figure and "$H_nE_2P \rightarrow H_nE_2$" corresponding to the *lower panels*). The initial level of phosphorylation corresponding to the regression line was taken as 100%.

Scheme 1), the enzyme was phosphorylated from [γ-^{32}P]ATP in the presence of 10 μM Ca^{2+} under conditions (0 °C, presence of 80 mM K^+, neutral pH) known to make the $Ca_2E_1P \rightarrow E_2P$ transition rate-limiting for the dephosphorylation in the SERCA1a and SERCA2b wildtypes, thus leading to accumulation of Ca_2E_1P (15, 20). To follow the dephosphorylation of E_1PCa_2 through the $Ca_2E_1P \rightarrow Ca_2E_2P \rightarrow E_2P \rightarrow H_nE_2P \rightarrow H_nE_2$ reaction sequence (*cf.* Scheme 1), the phosphoenzyme was chased by removing Ca^{2+} with excess EGTA, thereby preventing rephosphorylation (Fig. 5, *upper panels*, *circles*, and Table 3 column designated "$Ca_2E_1P \rightarrow E_2P$"). The observed dephosphorylation rate was ~1.7-fold enhanced for SERCA2b E917K compared with the wildtype SERCA2b, whereas it was about 2-fold slower in SERCA1a E918K and E918A than in the SERCA1a wildtype. These data confirm the isoform-specific mutational effects on k_B deduced by the computational analysis of the phosphorylation time course described above. Because of the rate limitation of the dephosphorylation imposed by the $Ca_2E_1P \rightarrow E_2P$ transition, the observed dephosphorylation time course reflects $Ca_2E_1P \rightarrow E_2P$ and not $H_nE_2P \rightarrow H_nE_2$. To verify that prior to the EGTA chase all of the accumulated phosphoenzyme really was the Ca_2E_1P species, which is ADP sensitive, unlike the ADP-insensitive E_2P, an experiment was carried out in which ADP was added together with EGTA allowing Ca_2E_1P to react backwards with ADP to form ATP and dephosphorylated Ca_2E_1, which resulted in almost complete dephosphorylation within 5 s both in wildtypes and mutants (Fig. 5, *upper panels*, *triangles*).

One of the factors ensuring that $Ca_2E_1P \rightarrow E_2P$ is rate-limiting for the dephosphorylation just described is the presence of 80 mM K^+, which accelerates the $H_nE_2P \rightarrow H_nE_2$ step (36). $H_nE_2P \rightarrow H_nE_2$ is slower at low K^+ concentration, allowing analysis of this reaction, as well. Incubation of the enzyme with $^{32}P_i$ in the absence of Ca^{2+} at acid pH and in the presence of the organic solvent dimethyl sulfoxide leads to accumulation of radioactively labeled H_nE_2P formed backwards from H_nE_2. The enzyme phosphorylated in this way was chased by addition of non-radioactive P_i and dilution in dimethyl sulfoxide-free medium of neutral pH and a low K^+ concentration (Fig. 5, *lower panels*). Under these conditions, SERCA2b E917K exhibited a 3-fold faster dephosphorylation, *i.e.* rate of $H_nE_2P \rightarrow H_nE_2$, than the SERCA2b wildtype, whereas SERCA1a E918K and E918A showed dephosphorylation rates similar to that of the SERCA1a wildtype (Fig. 5, *lower panels*, and Table 3 column designated "$H_nE_2P \rightarrow H_nE_2$").

The Ca^{2+}-binding transition of the dephosphoenzyme $H_nE_2 \rightarrow Ca_2E_1$ (*i.e.* $H_nE_2 \rightarrow H_nE_1 \rightarrow E_1 \rightarrow Ca_2E_1$ in Scheme 1) was studied at 25 °C using the quenched-flow module. The enzyme was preincubated in the absence of Ca^{2+} at pH 6.0, leading to accumulation of H_nE_2, followed by addition of Ca^{2+} to initiate the transition to Ca_2E_1. The time course of formation of Ca_2E_1 was observed by adding [γ-^{32}P]ATP at various time intervals followed in each case by quenching 34 ms later, thus taking advantage of the exclusive ability of Ca_2E_1 to become phosphorylated by ATP. Under these conditions the appearance of phosphorylated Ca_2E_1P enzyme reflects the appearance of Ca_2E_1 (35). Using the same method, we have previously found that the Ca^{2+}-binding transition is markedly slower in the SERCA2b wildtype as compared with SERCA2a and SERCA1a wildtypes (20), and the lower rate of the SERCA2b wildtype was confirmed here. The rate observed for SERCA2b E917K was slightly enhanced relative to the SERCA2b wildtype (0.38 ± 0.03 *versus* 0.30 ± 0.01 s^{-1}), whereas SERCA1a E918K was slower by 2-fold than the SERCA1a wildtype, thus approaching the rate of the SERCA2b wildtype (Fig. 6, *upper panels*, and Table 3 column designated "$H_nE_2 \rightarrow Ca_2E_1$").

The pH of 6.0 applied in the experiment just described ensures that in the wildtypes the proton release step $H_nE_2 \rightarrow H_nE_1 \rightarrow E_1$ is rate-limiting for the reaction sequence leading to Ca_2E_1. The evidence that such a proton release step exists and becomes rate-limiting at low pH (37) is in line with the proton counter transport steps shown in Scheme 1. To obtain information on the step involved directly in the binding of Ca^{2+} after the release of protons, *i.e.* $E_1 \rightarrow Ca_2E_1$, we increased the pH to 7.0, thereby allowing E_1 to accumulate during the pre-incubation in the absence of Ca^{2+} (37). Under these conditions both SERCA2b E917K and SERCA1a E918K displayed a reduced rate of phosphoenzyme appearance relative to the wildtype, 4- and 2.7-fold, respectively (Fig. 6, *lower panels*, and Table 3 column designated "$E_1 \rightarrow Ca_2E_1$"). This finding is in accordance with the transient kinetic analysis of the phosphorylation time course, indicating a reduced k_C for both SERCA2b E917K and SERCA1a E918K relative to the corresponding wildtype at pH

Table 3

Rate constants of partial reactions determined directly by measuring kinetics of phosphorylation and dephosphorylation

Rate constants ± S.D. were extracted from the data in Figs. 5 and 6 and data from similar experiments with E918A, R836A, and R835A by non-linear regression curve fitting as described in the figure legends. The number of independent experiments from which the data are derived is indicated as *n*. ND means not determined.

	$Ca_2E_1P \rightarrow E_2P$	*n*	$H_nE_2P \rightarrow H_nE_2$	*n*	$H_nE_2 \rightarrow Ca_2E_1$ (pH 6.0)	*n*	$E_1 \rightarrow Ca_2E_1$ (pH 7.0)	*n*
	s^{-1}		s^{-1}		s^{-1}		s^{-1}	
SERCA1a								
WT	0.14 ± 0.04	17	0.10 ± 0.01	7	0.83 ± 0.15	8	5.2 ± 0.48	2
E918K	0.07 ± 0.01	4	0.09 ± 0.02	2	0.38 ± 0.16	4	1.9 ± 0.14	2
E918A	0.06 ± 0.003	2	0.12 ± 0.01	2	ND		ND	
R836A	0.16 ± 0.03	4	0.44 ± 0.18	4	0.18 ± 0.07	2	ND	
SERCA2b								
WT	0.06 ± 0.01	3	0.02 ± 0.01	5	0.30 ± 0.01	2	1.4 ± 0.21	2
E917K	0.10 ± 0.02	2	0.06 ± 0.01	3	0.38 ± 0.03	3	0.34 ± 0.16	2
R835A	0.16 ± 0.03	6	0.12 ± 0.04	4	0.12 ± 0.02	2	ND	

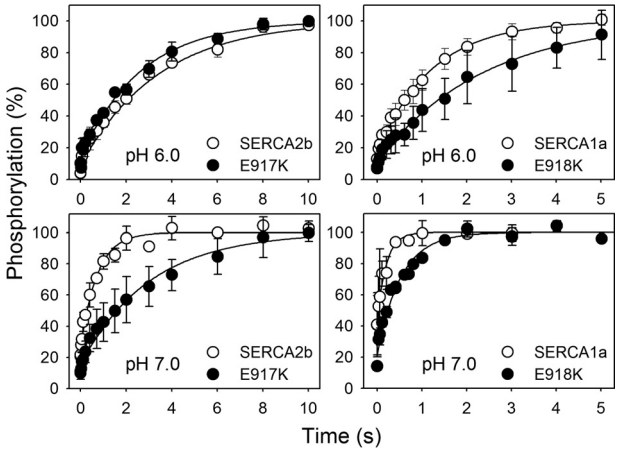

Figure 6. Kinetics of the Ca^{2+}-binding transition at pH 6.0 (*upper panels*) and pH 7.0 (*lower panels*). Quenched-flow experiments were carried out using a BioLogic QFM-5 module at 25 °C. For experiments at pH 6.0, the enzyme, preincubated in medium containing 40 mM MES/Tris (pH 6.0), 80 mM KCl, and 2 mM EGTA (to remove Ca^{2+}), was mixed with an equal volume of medium containing 40 mM MES/Tris (pH 6.0), 80 mM KCl, and 2.2 mM $CaCl_2$. At the indicated times, the amount of phosphorylatable Ca_2E_1 was determined by adding the double volume of 40 mM MES/Tris (pH 6.0), 80 mM KCl, 10 mM $MgCl_2$, 1 mM EGTA, 10 μM [γ-^{32}P]ATP, and 1.1 mM $CaCl_2$, followed by acid quenching 34 ms later. To obtain the point corresponding to zero time, the enzyme was pre-incubated in medium containing 40 mM MES/Tris (pH 6.0), 80 mM KCl, and 2 mM EGTA and mixed with an equal volume of 40 mM MES/Tris (pH 6.0), 80 mM KCl, 10 mM $MgCl_2$, 10 μM [γ-^{32}P]ATP, and 2.2 mM $CaCl_2$, followed by acid quenching 34 ms later. For experiments at pH 7.0, the 40 mM MES/Tris (pH 6.0) was replaced by 40 mM MOPS/Tris (pH 7.0). Error bars (seen only when larger than the size of the symbols) indicate S.D. The *lines* represent the best fits of a monoexponential "rise to max" function with an initial offset (*o*): $EP = (EP_{max} - o)\cdot(1 - e^{-k\cdot t}) + o$, giving the rate constants listed with statistics in Table 1 ("$H_nE_2 \rightarrow Ca_2E_1$" corresponding to the *upper panels* of this figure and "$E_1 \rightarrow Ca_2E_1$" corresponding to the *lower panels*). See a previous description of this analysis (43) for the rationale of the offset. In each case, the phosphorylation level at infinite time extracted from the fit was taken as 100%.

7.0 (Fig. 4 and Table 2). Because the rate of the $E_1 \rightarrow Ca_2E_1$ step was only 0.34 s^{-1} in SERCA2b E917K, it is clear that in this mutant the $E_1 \rightarrow Ca_2E_1$ step contributes very significantly to rate limitation of the Ca^{2+}-binding transition $H_nE_2 \rightarrow H_nE_1 \rightarrow E_1 \rightarrow Ca_2E_1$ at pH 7.0. The slightly increased rate of the complete transition described above for SERCA2b E917K at pH 6.0 seems therefore to be due to a balance between the reduced rate of $E_1 \rightarrow Ca_2E_1$ and an acceleration of the $H_nE_2 \rightarrow H_nE_1 \rightarrow E_1$ step. Hence, the acceleration is likely more prominent than immediately apparent from the rate constant determined at pH 6.0, and it may be concluded from this analysis that the effects of E917K/E918K on the conformational transition $H_nE_2 \rightarrow E_1$ in SERCA2b and SERCA1a are opposite, relieving inhibition in the former isoform and causing inhibition in the latter, whereas in both isoforms the $E_1 \rightarrow Ca_2E_1$ step is slowed by the mutation.

Analysis of SERCA2a and SERCA2b R835A and SERCA1a R836A mutants

The functional consequences of replacing Arg-835 in SERCA2a and SERCA2b and the corresponding Arg-836 in SERCA1a with alanine were studied as well, because Arg-835/836 seems to interact with Glu-917/918 (Fig. 7). The same strategy as described for the other mutants above was applied, characterizing first the overall reaction and then the rates of the partial reaction steps. SERCA2b R835A greatly enhanced the maximal turnover rate of ATPase activity and Ca^{2+} transport relative to wildtype SERCA2b, in fact more than seen for E917K. For SERCA2a and SERCA1a, this mutation also enhanced the turnover rate, but to a lesser extent. Like E917K/E918K, the R835/836A mutation reduced the apparent Ca^{2+} affinity and increased the apparent affinity for vanadate significantly in all three isoforms (Table 1). These results were supported by analysis of the transient kinetics of phosphorylation of the R835/836A mutants performed as for Fig. 3, showing for all three mutants a significant enhancement of k_B, which was most pronounced for SERCA2b, and reduction of k_C, relative to the corresponding wildtype (Table 2), which should lead to accumulation of the vanadate-reactive form, H_nE_2, during enzyme turnover at steady state, thus explaining the increased apparent affinity for vanadate.

Using the same procedures as for Figs. 5 and 6, the rates of the partial reactions were determined directly for SERCA1a R836A and SERCA2b R835A (Table 3). The $Ca_2E_1P \rightarrow E_2P$ transition was wildtype-like in SERCA1a R836A, but was markedly enhanced in SERCA2b R835A relative to the SERCA2b wildtype. The rate of the $H_nE_2P \rightarrow H_nE_2$ dephosphorylation step showed 4- and 6-fold increases in SERCA1a R836A and SERCA2b R835A, respectively. Furthermore, R836A/R835A reduced the rate of the $H_nE_2 \rightarrow Ca_2E_1$ transition markedly in both isoforms.

Discussion

Prompted by the finding that a sporadic mutation changing Glu-917 of SERCA2b to lysine causes DD (32), we have studied the functional consequences of this mutation and the corresponding mutations in SERCA2a and SERCA1a. In DD, the epidermal keratinocytes are prone to develop endoplasmic

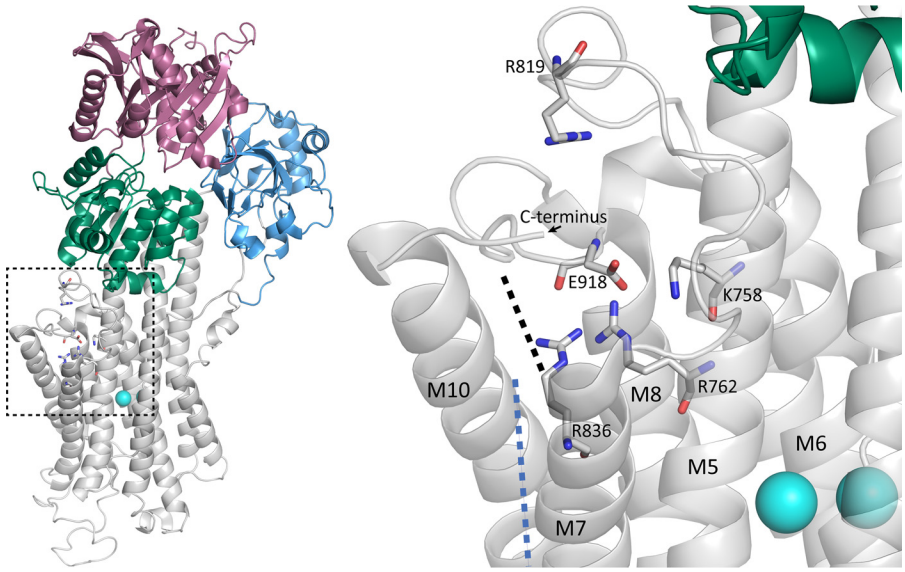

Figure 7. Structural features of SERCA1a relevant to the present findings. Overview (*left*) and close up (*right*) of the structure corresponding to the Protein Data Bank accession code 3N8G (SERCA1a with bound Ca^{2+} and AMPPCP). The A-, P-, and N-domains are colored *blue*, *green*, and *pink*, respectively. The membrane helices are *gray*. The two Ca^{2+} ions are shown as *cyan spheres*. *Dashed square* indicates the part shown as a close-up to the *right*, with Glu-918 located in the center. In the close-up, two possible positions of TM11, on each side of TM10, are indicated by *dashed lines*, in *black* on the "TM8 side" and in *blue* on the "TM7 side."

reticulum stress response with resulting apoptosis and characteristic dyskeratotic features. As part of this complex process, defective SERCA2b function leads to endoplasmic reticulum Ca^{2+} store depletion of the keratinocytes (26) with consequences for Ca^{2+} signaling at various levels, including changes in the expression levels of various proteins involved, such as store-operated Ca^{2+} channels (38). Using the mammalian COS-1 cell expression systems, we have found both a 5-fold reduced expression level and a reduced apparent Ca^{2+} affinity of the DD mutant E917K as compared with the wildtype SERCA2b. Assuming that in the patients the mutation reduces the expression level of SERCA2b in the keratinocytes to a similar extent as seen for the COS-1 cells, the net effect of the mutation on the endoplasmic reticulum Ca^{2+} uptake may well be a decrease, in line with current views on the pathophysiological mechanism (26, 38). However, we also found that the E917K mutation leads to a 30–50% increase of the maximal turnover rates of ATPase activity and Ca^{2+} transport determined at saturating Ca^{2+} concentration. Because the Ca^{2+} levels can become quite high in restricted subcellular microdomains, and the spatial extent and temporal persistence of Ca^{2+} signals may be significantly shaped by subpopulations of SERCA operating at high or even saturating Ca^{2+}, it cannot be excluded that the increased maximal turnover rate contributes to the pathophysiology.

The increased maximal turnover rate observed for SERCA2b E917K, relative to the wildtype SERCA2b, is isoform-specific and dependent on the presence of the SERCA2b tail, because the equivalent SERCA2a and SERCA1a mutants instead showed reduced maximal turnover rates relative to the corresponding wildtypes. Therefore, our observation sheds new light on the structure–function relationship that determines the kinetic constraints imposed by the SERCA2b tail. Our analysis of the partial reaction steps showed for SERCA2b E917K increased rate of both the $Ca_2E_1P \rightarrow E_2P$ transition and the $H_nE_2P \rightarrow H_nE_2$ dephosphorylation step (Table 3). Either of these steps contributes to rate limitation of the overall reaction at the conditions applied for measurement of maximal turnover of ATPase activity and Ca^{2+} transport (15, 39). On the contrary, the E918K mutation in SERCA1a markedly slowed the $Ca_2E_1P \rightarrow E_2P$ transition, thus explaining the reduced maximal turnover rate of the SERCA1a mutant. In SERCA1a, the mutation was without effect on the rate of $H_nE_2P \rightarrow H_nE_2$ (Table 3). Another isoform-specific difference that appears from our analysis is that in SERCA2b the mutation E917K caused acceleration of the $H_nE_2 \rightarrow E_1$ step of the Ca^{2+}-binding transition of the dephosphoenzyme, whereas in SERCA1a E918K, we found $H_nE_2 \rightarrow E_1$ slower than in the corresponding wildtype. This step is not likely to contribute to rate limitation of the overall reaction at the neutral pH and millimolar ATP concentration present during measurements of ATPase activity and Ca^{2+} transport (39), but the acceleration of $H_nE_2P \rightarrow H_nE_2$ by E917K constitutes yet another example of relief of the inhibitory influence of the SERCA2b tail caused by the E917K mutation. It was previously found that the presence of the SERCA2b tail slows the phosphoenzyme-processing steps $Ca_2E_1P \rightarrow E_2P$ and $H_nE_2P \rightarrow H_nE_2$ as well as the $H_nE_2 \rightarrow E_1$ step of the Ca^{2+}-binding transition, and that the two main parts of the SERCA2b tail, the 11th transmembrane helix (TM11) and the associated 11-amino acid LE, play differential roles in the inhibition, with the TM11 contributing to the slowing of all the three steps mentioned and the LE contributing only to the slowing of $Ca_2E_1P \rightarrow E_2P$ (20). Hence, it is clear that the relief of the inhibition by the SERCA2b tail caused by the E917K mutation can be ascribed to an influence on the interaction of TM11, whereas the interaction of the LE may or may not be influenced by the mutation.

In the absence of X-ray crystallographic evidence, there are two possibilities for the location of TM11 in SERCA2b, as judged from the known SERCA1a structure (Fig. 7). Either

TM11 is on "the TM7 side" or it is on "the TM8 side" of TM10 (*blue* and *black dashed lines*, respectively, in Fig. 7). Based on functional effects of mutations in TM7 and TM10, a structural model of SERCA2b was previously generated, where TM11 was docked at the TM7 side of TM10 (18, 19). In this study, we found that mutation of the arginine residue in TM7 (Arg-835 in SERCA2a/2b and Arg-836 in SERCA1a) caused effects in SERCA2b reminiscent of those of E917K, further pointing to a role of TM7 in the TM11 inhibition mechanism. The acceleration of $Ca_2E_1P \rightarrow E_2P$ by the R835A mutation, in particular, is unique for SERCA2b, not being seen for R836A in SERCA1a (Table 3). In the SERCA1a crystal structures (both E_1 and E_2 states), this arginine seems to interact closely with the Glu-918 backbone carbonyl group. Hence, the interaction of Arg-835 with Glu-917 could be instrumental in mediating the slowing of $Ca_2E_1P \rightarrow E_2P$ by TM11 in wildtype SERCA2b, which according to our data is relieved by mutation E917K or R835A, either of which is expected to disrupt the bond between them (in case of E917K, the drastic change of side chain would probably move the backbone). Hence, the arginine side chain may work as a brake on the $Ca_2E_1P \rightarrow E_2P$ conformational transition in the presence of the TM11. Such a mechanism would require TM7 to be functionally linked with TM11. Irrespective of whether TM11 is on the TM7 side or on the TM8 side of TM10, it is likely that the luminal extension of TM11 interacts with the luminal loop between TM7 and TM8 (18, 20), an interaction that might be disturbed by changes to TM7.

It is also very likely that the E917K mutation affects the position of TM11 through interaction of the lysine side chain with residue(s) in the nearby cytoplasmic loop connecting TM10 and TM11 ("L10–11"). Hence, in the crystal structure of SERCA1a, the C-terminal glycine of SERCA1a would clearly be within reach of the side chain of a lysine substituent at the position of Glu-918 (*cf.* Fig. 7, "C terminus"). Previous results obtained with another DD mutation, S920Y (15), support such a mechanism. Of the more than 50 Darier disease mutations so far analyzed functionally (15, 30, 39, 40), only S920Y caused in addition to reduced Ca^{2+} affinity and expression level also the acceleration of the phosphoenzyme processing steps similarly to E917K (15). Ser-920 is located only three residues from Glu-917 in the same cytoplasmic loop between TM8 and TM9 ("L8–9"). Like E917K, the S920Y mutation has a potential for disturbing L10–11 and thereby the TM11 path due to the introduction of the bulky tyrosine.

One of our present findings with the Glu-917/918 mutants is not isoform-specific, namely the reduced affinity for Ca^{2+} binding to E_1, which was observed for all three isoforms. The data suggest that the reduced Ca^{2+} affinity is due to a reduced rate of the $E_1 \rightarrow Ca_2E_1$ transition (Table 3). Because of its lack of isoform specificity, this effect may for all isoforms be rationalized on the basis of the SERCA1a structure and mutagenesis results. The SERCA1a crystal structures show Glu-918 surrounded by several arginine and lysine residues positioned with a potential for ionic interaction or hydrogen bonding with the Glu-918 side-chain carboxyl group or backbone carbonyl oxygen (Fig. 7). Thus, in addition to Arg-836 (TM7), also Lys-758 (TM5), Arg-762 (TM5), and Arg-819 (cytoplasmic loop between TM6 and TM7) could be involved in functionally important interactions with Glu-918. Previous mutagenesis of SERCA1a Lys-758 (41), Arg-762 (42), and Arg-819 (43) has also given rise to reduced Ca^{2+} affinity and kinetics compatible with a defective $E_1 \rightarrow Ca_2E_1$ transition. It is therefore quite likely that the cause of this defect is interference with the intricate bonding network centered around Glu-918. TM5 contains residues that are directly involved in Ca^{2+} binding, and the conformational rearrangements of the Ca^{2+} sites responsible for the cooperative binding of Ca^{2+} during the $E_1 \rightarrow Ca_2E_1$ transition include a straightening of the bent TM5 helix (4). Hence, the linking of Glu-918 to the two TM5 residues Lys-758 and Arg-762, which is disrupted by mutation of these residues, may be important in the mechanism of Ca^{2+} binding. In addition, the function of the Ca^{2+}-binding residues in TM6 (4) might be influenced by a change of the position of the loop between TM6 and TM7, and indirectly by the position of TM7, thus making the links of Arg-819 and Arg-836 to Glu-918 important for Ca^{2+} binding.

Conclusions

The most likely reason that the SERCA2b E917K mutation reduces the endoplasmic reticulum Ca^{2+} uptake, thereby causing DD, is a reduced expression level in keratinocytes, similar to that observed here for COS-1 cells. The unexpected SERCA2b-specific increase of the maximal turnover rate observed for the DD mutant is due to a relief of the kinetic constraints of specific partial reactions imposed by the TM11. This relief is caused by disturbance of the interaction of Glu-917 with Arg-835 of TM7 and likely also by an effect on TM11 mediated through the cytoplasmic loop L10–11.

Experimental procedures

Mutations were introduced in cDNA encoding SERCA1a, SERCA2a, and SERCA2b (8, 9) in the pMT2 expression vector (44) using the QuikChange site-directed mutagenesis kit (Agilent Technologies). The wildtypes and mutants were transiently expressed in COS-1 cells using the calcium phosphate precipitation method for transfection (45). Harvest of microsomal vesicles containing SERCA enzyme was carried out by differential centrifugation (46). The concentration of expressed active SERCA enzyme was determined by measuring the maximum phosphorylation capacity with either [γ-^{32}P]ATP or $^{32}P_i$ under stoichiometric phosphorylation conditions (41). Ca^{2+}-ATPase activity was determined under the conditions described in the figure legends by following the liberation of P_i at 37 °C using the Baginski method (47) over 10 min, which is within the linear time range (41). The rate of ATP-driven $^{45}Ca^{2+}$ uptake in the isolated endoplasmic reticulum vesicles was determined by filtration, following incubation of the microsomal vesicles for 5 min at 37 °C in medium containing 5 mM ATP, 20 mM MOPS/Tris (pH 6.8), 100 mM KCl, 5 mM $MgCl_2$, 0.5 mM EGTA, 0.45 mM $^{45}CaCl_2$ (corresponding to 5 μM free Ca^{2+}), and 5 mM potassium oxalate (to precipitate and thereby trap Ca^{2+} accumulated at high concentration inside the vesicles) (48).

Phosphorylation experiments using [γ-^{32}P]ATP or $^{32}P_i$ to analyze the partial reactions of the Ca^{2+}-ATPase reaction cycle were carried out as described previously (15, 20, 35, 48), either

by manual mixing at 0 °C or at 25 °C using a Bio-Logic quench-flow module QMF-5 (Bio-Logic Science Instruments, Claix, France). Following acid-quenching and acid SDS-PAGE, the radioactivity associated with the separated Ca^{2+}-ATPase band was quantified by phosphorimaging using a Cyclone storage phosphor system (PerkinElmer Life Sciences). Further details of the experimental conditions are given in the figure legends.

All experiments were conducted at least twice on independent samples (see *n* values in tables), and average values are shown on the graphs, with *error bars* (seen only when larger than the size of the symbols) representing standard deviation (S.D.). Non-linear regression analysis was carried out using the SigmaPlot program (SPSS, Inc.), and extracted parameters with statistics are reported in the tables.

The non-monoexponential time courses of phosphorylation were analyzed using the program SimZyme to determine the rate constants by "trial and error" in kinetic simulation of the reaction cycle (35). The rate constants were varied, until an optimal fit to the data points was obtained. For any choice of reaction cycle and rate constants, the SimZyme program solves the relevant differential equations numerically and shows a graphical representation of the time dependence of the concentrations of the reaction intermediates. In this study, we compared the calculated time dependence of the concentration of phosphoenzyme with experimental data points corresponding to the phosphorylation time course.

Author contributions—S. A. M., P. V., and J. P. A. conceptualization; S. A. M. data curation; S. A. M. and J. P. A. formal analysis; S. A. M. and J. P. A. supervision; S. A. M. and J. P. A. validation; S. A. M., P. V., and J. P. A. investigation; S. A. M. and J. P. A. visualization; S. A. M. and J. P. A. methodology; S. A. M. writing-original draft; S. A. M., P. V., and J. P. A. writing-review and editing; J. P. A. resources; J. P. A. software; J. P. A. funding acquisition; J. P. A. project administration.

Acknowledgments—Karin Kracht and Lene Jacobsen (Aarhus University) provided expert technical assistance. We are also thankful to Dr. C. Toyoshima (University of Tokyo) for discussion of structure–function relationship and to Joren De Raeymaecker and Marc De Maeyer (KU Leuven) for molecular dynamics simulations.

References

1. Berridge, M. J., Lipp, P., and Bootman, M. D. (2000) The versatility and universality of calcium signalling. *Nat. Rev. Mol. Cell Biol.* **1,** 11–21 CrossRef Medline
2. Vandecaetsbeek, I., Vangheluwe, P., Raeymaekers, L., Wuytack, F., and Vanoevelen, J. (2011) The Ca^{2+} pumps of the endoplasmic reticulum and Golgi apparatus. *Cold Spring Harb. Perspect. Biol.* **3,** a004184 Medline
3. Pedersen, P. L., and Carafoli, E. (1987) Ion motive ATPases. I. Ubiquity, properties, and significance to cell function. *Trends Biochem. Sci.* **12,** 146–150 CrossRef
4. Toyoshima, C. (2008) Structural aspects of ion pumping by Ca^{2+}-ATPase of sarcoplasmic reticulum. *Arch. Biochem. Biophys.* **476,** 3–11 CrossRef Medline
5. Morth, J. P., Pedersen, B. P., Buch-Pedersen, M. J., Andersen, J. P., Vilsen, B., Palmgren, M. G., and Nissen, P. (2011) A structural overview of the plasma membrane Na^+,K^+-ATPase and H^+-ATPase ion pumps. *Nat. Rev. Mol. Cell Biol.* **12,** 60–70 CrossRef Medline
6. Bublitz, M., Poulsen, H., Morth, J. P., and Nissen, P. (2010) In and out of cation pumps: P-type ATPase structure revisited. *Curr. Opin. Struct. Biol.* **20,** 431–439 CrossRef Medline
7. MacLennan, D. H., Brandl, C. J., Korczak, B., and Green, N. M. (1985) Amino-acid sequence of a Ca^{2+} + Mg^{2+}-dependent ATPase from rabbit muscle sarcoplasmic reticulum, deduced from its complementary DNA sequence. *Nature* **316,** 696–700 CrossRef Medline
8. Lytton, J., and MacLennan, D. H. (1988) Molecular cloning of cDNAs from human kidney coding for two alternatively spliced products of the cardiac Ca^{2+}-ATPase gene. *J. Biol. Chem.* **263,** 15024–15031 Medline
9. Brandl, C. J., deLeon, S., Martin, D. R., and MacLennan, D. H. (1987) Adult forms of the Ca^{2+}-ATPase of sarcoplasmic reticulum. Expression in developing skeletal muscle. *J. Biol. Chem.* **262,** 3768–3774 Medline
10. Dally, S., Corvazier, E., Bredoux, R., Bobe, R., and Enouf, J. (2010) Multiple and diverse coexpression, location, and regulation of additional SERCA2 and SERCA3 isoforms in nonfailing and failing human heart. *J. Mol. Cell. Cardiol.* **48,** 633–644 CrossRef Medline
11. Lytton, J., Westlin, M., Burk, S. E., Shull, G. E., and MacLennan, D. H. (1992) Functional comparisons between isoforms of the sarcoplasmic or endoplasmic reticulum family of calcium pumps. *J. Biol. Chem.* **267,** 14483–14489 Medline
12. Verboomen, H., Wuytack, F., De Smedt, H., Himpens, B., and Casteels, R. (1992) Functional difference between SERCA2a and SERCA2b Ca^{2+} pumps and their modulation by phospholamban. *Biochem. J.* **286,** 591–595 CrossRef Medline
13. Verboomen, H., Wuytack, F., Van den Bosch, L., Mertens, L., and Casteels, R. (1994) The functional importance of the extreme C-terminal tail in the gene 2 organellar Ca^{2+}-transport ATPase (SERCA2a/b). *Biochem. J.* **303,** 979–984 CrossRef Medline
14. Dode, L., Vilsen, B., Van Baelen, K., Wuytack, F., Clausen, J. D., and Andersen, J. P. (2002) Dissection of the functional differences between sarco(endo)plasmic reticulum Ca^{2+}-ATPase (SERCA) 1 and 3 isoforms by steady-state and transient kinetic analyses. *J. Biol. Chem.* **277,** 45579–45591 CrossRef Medline
15. Dode, L., Andersen, J. P., Leslie, N., Dhitavat, J., Vilsen, B., and Hovnanian, A. (2003) Dissection of the functional differences between sarco(endo-)plasmic reticulum Ca^{2+}-ATPase (SERCA) 1 and 2 isoforms and characterization of Darier disease (SERCA2) mutants by steady-state and transient kinetic analyses. *J. Biol. Chem.* **278,** 47877–47889 CrossRef Medline
16. Yu, X., T., Hao, L., and Inesi, G. (1994) A pK change of acidic residues contributes to cation countertransport in the Ca-ATPase of sarcoplasmic reticulum. *J. Biol. Chem.* **269,** 16656–16661 Medline
17. Toyoshima, C., Nakasako, M., Nomura, H., and Ogawa, H. (2000) Crystal structure of the calcium pump of sarcoplasmic reticulum at 2.6 A resolution. *Nature* **405,** 647–655 CrossRef Medline
18. Vandecaetsbeek, I., Trekels, M., De Maeyer, M., Ceulemans, H., Lescrinier, E., Raeymaekers, L., Wuytack, F., and Vangheluwe, P. (2009) Structural basis for the high Ca^{2+} affinity of the ubiquitous SERCA2b Ca^{2+} pump. *Proc. Natl. Acad. Sci. U.S.A.* **106,** 18533–18538 CrossRef Medline
19. Gorski, P. A., Trieber, C. A., Larivière, E., Schuermans, M., Wuytack, F., Young, H. S., and Vangheluwe, P. (2012) Transmembrane helix 11 is a genuine regulator of the endoplasmic reticulum Ca^{2+} pump and acts as a functional parallel of β-subunit on α-Na^+,K^+-ATPase. *J. Biol. Chem.* **287,** 19876–19885 CrossRef Medline
20. Clausen, J. D., Vandecaetsbeek, I., Wuytack, F., Vangheluwe, P., and Andersen, J. P. (2012) Distinct roles of the C-terminal 11th transmembrane helix and luminal extension in the partial reactions determining the high Ca2+ affinity of sarco(endo)plasmic reticulum Ca^{2+}-ATPase isoform 2b (SERCA2b). *J. Biol. Chem.* **287,** 39460–39469 CrossRef Medline
21. Clarke, D. M., Loo, T. W., Inesi, G., and MacLennan, D. H. (1989) Location of high affinity Ca^{2+}-binding sites within the predicted transmembrane domain of the sarcoplasmic reticulum Ca^{2+}-ATPase. *Nature* **339,** 476–478 CrossRef Medline
22. Andersen, J. P., and Vilsen, B. (1992) Functional consequences of alterations to Glu309, Glu771, and Asp800 in the Ca^{2+}-ATPase of sarcoplasmic reticulum. *J. Biol. Chem.* **267,** 19383–19387 Medline

23. Andersen, J. P., and Vilsen, B. (1994) Amino acids Asn796 and Thr799 of the Ca^{2+}-ATPase of sarcoplasmic reticulum bind Ca^{2+} at different sites. *J. Biol. Chem.* **269,** 15931–15936 Medline
24. Møller, J. V., Olesen, C., Winther, A. M., and Nissen, P. (2010) The sarcoplasmic Ca^{2+}-ATPase: design of a perfect chemi-osmotic pump. *Q. Rev. Biophys.* **43,** 501–566 CrossRef Medline
25. Tavadia, S., Authi, K. S., Hodgins, M. B., and Munro, C. S. (2004) Expression of the sarco/endoplasmic reticulum calcium ATPase type 2 and 3 isoforms in normal skin and Darier's disease. *Br. J. Dermatol.* **151,** 440–445 CrossRef Medline
26. Savignac, M., Edir, A., Simon, M., and Hovnanian, A. (2011) Darier disease: a disease model of impaired calcium homeostasis in the skin. *Biochim. Biophys. Acta* **1813,** 1111–1117 CrossRef Medline
27. Sakuntabhai, A., Ruiz-Perez, V., Carter, S., Jacobsen, N., Burge, S., Monk, S., Smith, M., Munro, C. S., O'Donovan, M., Craddock, N., Kucherlapati, R., Rees, J. L., Owen, M., Lathrop, G. M., Monaco, A. P., Strachan, T., and Hovnanian, A. (1999) Mutations in ATP2A2, encoding a Ca^{2+} pump, cause Darier disease. *Nat. Genet.* **21,** 271–277 CrossRef Medline
28. Peacocke, M., and Christiano, A. M. (1999) Bumps and pumps, SERCA 1999. *Nat. Genet.* **21,** 252–253 CrossRef Medline
29. Nellen, R. G., Steijlen, P. M., van Steensel, M. A., Vreeburg, M., European Professional Contributors, Frank, J., and van Geel, M. (2017) Mendelian disorders of cornification caused by defects in intracellular calcium pumps: Mutation update and database for variants in ATP2A2 and ATP2C1 associated with Darier disease and Hailey-Hailey disease. *Hum. Mutat.* **38,** 343–356 CrossRef Medline
30. Miyauchi, Y., Daiho, T., Yamasaki, K., Takahashi, H., Ishida-Yamamoto, A., Danko, S., Suzuki, H., and Iizuka, H. (2006) Comprehensive analysis of expression and function of 51 sarco(endo)plasmic reticulum Ca^{2+}-ATPase mutants associated with Darier disease. *J. Biol. Chem.* **281,** 22882–22895 CrossRef Medline
31. Celli, A., Sanchez, S., Behne, M., Hazlett, T., Gratton, E., and Mauro, T. (2010) The epidermal Ca^{2+} gradient: measurement using the phasor representation of fluorescent lifetime imaging. *Biophys. J.* **98,** 911–921 CrossRef Medline
32. Ikeda, S., Mayuzumi, N., Shigihara, T., Epstein, E. H., Jr, Goldsmith, L. A., and Ogawa, H. (2003) Mutations in ATP2A2 in patients with Darier's disease. *J. Invest. Dermatol.* **121,** 475–477 CrossRef Medline
33. Cantley, L. C., Jr., Cantley, L. G., and Josephson, L. (1978) A characterization of vanadate interactions with the (Na,K)-ATPase. Mechanistic and regulatory implications. *J. Biol. Chem.* **253,** 7361–7368 Medline
34. Pick, U. (1982) The interaction of vanadate ions with the Ca-ATPase from sarcoplasmic reticulum. *J. Biol. Chem.* **257,** 6111–6119 Medline
35. Sorensen, T. L., Dupont, Y., Vilsen, B., and Andersen, J. P. (2000) Fast kinetic analysis of conformational changes in mutants of the Ca^{2+}-ATPase of sarcoplasmic reticulum. *J. Biol. Chem.* **275,** 5400–5408 CrossRef Medline
36. Sørensen, T. L., Clausen, J. D., Jensen, A.-M., Vilsen, B., Møller, J. V., Andersen, J. P., and Nissen, P. (2004) Localization of a K^+-binding site involved in dephosphorylation of the sarcoplasmic reticulum Ca^{2+}-ATPase. *J. Biol. Chem.* **279,** 46355–46358 CrossRef Medline
37. Forge, V., Mintz, E., and Guillain, F. (1993) Ca^{2+} binding to sarcoplasmic reticulum ATPase revisited. II. Equilibrium and kinetic evidence for a two-route mechanism. *J. Biol. Chem.* **268,** 10961–10968 Medline
38. Pani, B., and Singh, B. B. (2008) Darier's disease: a calcium-signaling perspective. *Cell. Mol. Life Sci.* **65,** 205–211 CrossRef Medline
39. Champeil, P., le Maire, M., Andersen, J. P., Guillain, F., Gingold, M., Lund, S., and Møller, J. V. (1986) Kinetic characterization of the normal and detergent-perturbed reaction cycles of the sarcoplasmic reticulum calcium pump. Rate-limiting step(s) under different conditions. *J. Biol. Chem.* **261,** 16372–16384 Medline
40. Sato, K., Yamasaki, K., Daiho, T., Miyauchi, Y., Takahashi, H., Ishida-Yamamoto, A., Nakamura, S., Iizuka, H., and Suzuki, H. (2004) Distinct types of abnormality in kinetic properties of three Darier disease-causing sarco(endo)plasmic reticulum Ca^{2+}-ATPase mutants that exhibit normal expression and high Ca^{2+} transport activity. *J. Biol. Chem.* **279,** 35595–35603 CrossRef Medline
41. Sorensen, T., Vilsen, B., and Andersen, J. P. (1997) Mutation Lys-758 → Ile of the sarcoplasmic reticulum Ca^{2+}-ATPase enhances dephosphorylation of E_2P and inhibits the E_2 to E_1Ca_2 transition. *J. Biol. Chem.* **272,** 30244–30253 CrossRef Medline
42. Sorensen, T. L., and Andersen, J. P. (2000) Importance of stalk segment S5 for intramolecular communication in the sarcoplasmic reticulum Ca^{2+}-ATPase. *J. Biol. Chem.* **275,** 28954–28961 CrossRef Medline
43. Clausen, J. D., and Andersen, J. P. (2004) Functional consequences of alterations to Thr247, Pro248, Glu340, Asp813, Arg-819, and Arg822 at the interfaces between domain P, M3, and L6–7 of sarcoplasmic reticulum Ca^{2+}-ATPase. Roles in Ca^{2+} interaction and phosphoenzyme processing. *J. Biol. Chem.* **279,** 54426–54437 CrossRef Medline
44. Kaufman, R. J., Davies, M. V., Pathak, V. K., and Hershey, J. W. (1989) The phosphorylation state of eucaryotic initiation factor 2 alters translational efficiency of specific mRNAs. *Mol. Cell. Biol.* **9,** 946–958 CrossRef Medline
45. Chen, C., and Okayama, H. (1987) High-efficiency transformation of mammalian cells by plasmid DNA. *Mol. Cell. Biol.* **7,** 2745–2752 CrossRef Medline
46. Maruyama, K., and MacLennan, D. H. (1988) Mutation of aspartic acid-351, lysine-352, and lysine-515 alters the Ca^{2+} transport activity of the Ca^{2+}-ATPase expressed in COS-1 cells. *Proc. Natl. Acad. Sci. U.S.A.* **85,** 3314–3318 CrossRef Medline
47. Baginski, E. S., Foà, P. P., and Zak, B. (1967) Microdetermination of inorganic phosphate, phospholipids, and total phosphate in biologic materials. *Clin. Chem.* **13,** 326–332 Medline
48. Vilsen, B., Andersen, J. P., Clarke, D. M., and MacLennan, D. H. (1989) Functional consequences of proline mutations in the cytoplasmic and transmembrane sectors of the Ca^{2+}-ATPase of sarcoplasmic reticulum. *J. Biol. Chem.* **264,** 21024–21030 Medline